Tricarbon Carborane Chemistry. 2. Syntheses and Structural Characterizations of Commo Iron and Cobalt Bis(tricarbaborane) Complexes

Carole A. Plumb, Patrick J. Carroll, and Larry G. Sneddon*

Department of Chemistry, University of Pennsylvania, Philadelphia, Pennsylvania 19104

Received October 29, 1991

A series of commo metalla bis(tricarbaborane) complexes has been generated via the reaction of the metal halide with the 6-CH_3-5,6,9-$C_3B_7H_9^-$ anion. Reaction of 6-CH_3-5,6,9-$C_3B_7H_9^-$ with $FeCl_2$ yielded the isomeric complexes *commo-Fe*-(1-Fe-2-CH_3-2,3,5-$C_3B_7H_9$)$_2$ (**6**), *commo-Fe*-(1-Fe-5-CH_3-2,3,5-$C_3B_7H_9$)$_2$ (**7**), and *commo-Fe*-(1-Fe-5-CH_3-2,3,5-$C_3B_7H_9$)(1-Fe-4-CH_3-2,3,4-$C_3B_7H_9$) (**8**). Thermolysis of **6**, **7**, or **8** was found to produce a new isomer, *commo-Fe*-(1-Fe-10-CH_3-2,3,10-$C_3B_7H_9$)$_2$ (**9**). Single-crystal X-ray determinations of **6**–**9** have confirmed that in each structure the iron atom is sandwiched between two tricarbon carborane cages. Compounds **6** and **7** differ in the site of substitution of the exopolyhedral methyl group. In **6** the methyl group is bound to a four-coordinate carbon as in the 6-CH_3-5,6,9-$C_3B_7H_9^-$ anion. In **7** the methyl group has rearranged to an adjacent five-coordinate cage carbon. Variable-temperature NMR studies of **7** also indicate that it is fluxional in solution. In **8**, like **7**, a methyl rearrangement to the five-coordinate carbon has occurred, but unlike **7**, the two tricarbon carborane cages are of two different enantiomeric forms. In **9**, a cage-carbon rearrangement has maximized the separation of the skeletal carbons. Although the ferratricarbaborane fragments Fe(CH_3)$C_3B_7H_9$ in **6**–**9** each exhibit gross octadecahedral geometries consistent with their closo 24-skeletal-electron counts, **6**–**8** also show cage distortions that result in the formation of open four-membered Fe–C–C–B faces. Reaction of 6-CH_3-5,6,9-$C_3B_7H_9^-$ with $CoCl_2$ yielded two compounds, *commo-Co*-(1-Co-2-CH_3-2,3,5-$C_3B_7H_9$)(1-Co-5-CH_3-2,3,5-$C_3B_7H_9$) (**10**) and *commo-Co*-(1-Co-2-CH_3-2,3,5-$C_3B_7H_9$)$_2$ (**11**). Both **10** and **11** are 19-electron, air-stable analogues of cobaltocene, and their structures were established by single-crystal X-ray studies. Both compounds have sandwich structures, but the cage units show cage distortions resulting in open structures that are intermediate between the normal 11-vertex 24-skeletal-electron closo and 26-skeletal-electron nido structures.

Introduction

In the preceding paper,[1] we reported the series of metalla monocage tricarbaborane complexes **2**–**5**, derived from the 6-CH_3-5,6,9-$C_3B_7H_9^-$ anion. In this paper the metal chemistry of this tricarbon carborane anion is further extended and the syntheses of a series of new commo iron and cobalt bis(tricarbaborane) complexes that are analogues of ferrocene and cobaltocene are reported.[2] Structural characterizations of these complexes have revealed several unique features, including cage distortions in the ferratricarbaborane complexes that may result from the nonconical nature of the $CH_3C_3B_7H_9^-$ ligand, a cage rearrangement reaction leading to apparent methyl-migrated isomers, and, in the cobaltatricarbaboranes, open-cage structures that are intermediate between those expected for 11-vertex nido and closo skeletal-electron counts.

Experimental Section

All experimental manipulations were carried out using standard high-vacuum or inert-atmosphere techniques as described by Shriver.[3]

Materials. A modified synthesis[4] was used for Na^+(6-CH_3-5,6,9-$C_3B_7H_9$)$^-$ as described in the preceding paper.[1] $FeCl_2$ was prepared according to previously reported methods[5] and stored under an inert atmosphere until use. $CoCl_2$ was dried for 12 h at 100 °C in vacuo and stored under an inert atmosphere until used. Spectrochemical grade CH_3CN, THF, Et_2O, and CH_2Cl_2 were purchased from Fisher or EM Science. Degassed THF and Et_2O were stored over sodium–benzophenone ketyl until used. CH_2Cl_2 was dried over P_2O_5, transferred onto activated 4-Å molecular sieves, and stored under vacuum until used. Anhydrous CH_3CN was stored over activated 4-Å molecular sieves. All other reagents were commercially obtained and used as received unless noted otherwise.

Physical Measurements. ^{11}B NMR spectra at 160.5 MHz, ^{13}C NMR spectra at 125.7 MHz, and ^1H NMR spectra at 500 MHz were obtained on a Bruker AM-500 spectrometer equipped with the appropriate decoupling accessories. ^{11}B NMR spectra at 64.2 MHz, ^{13}C NMR spectra at 50.3 MHz, and ^1H NMR spectra at 200 MHz were obtained on a Bruker AC-200 spectrometer equipped with the appropriate decoupling accessories. All ^{11}B chemical shifts were referenced to $BF_3{\cdot}O(C_2H_5)_2$ (0.0 ppm) with a negative sign indicating an upfield shift. All proton chemical shifts were measured relative to internal residual protons from the lock solvent (99.5% C_6D_6 or $CD_3C_6D_5$) and then referenced to $(CH_3)_4Si$ (0.0 ppm). Two-dimensional COSY ^{11}B–^{11}B experiments were performed at 160.5 MHz using the procedures described[6] previously. NMR data are presented in Table I.

Effective magnetic moments were measured by the solution method of Evans.[7] EPR spectra were obtained at 9.41 GHz on a Bruker ER 100D instrument at 77 K in a toluene glass referenced to DPPH.

High- and low-resolution mass spectra were obtained on a VG-ZAB-E high-resolution mass spectrometer. Infrared spectra were obtained on a Perkin-Elmer 1430 spectrophotometer. A Hewlett-Packard 8452A diode array spectrophotometer was used to obtain ultraviolet–visible spectra. Cyclic voltammetric measurements were performed under argon gas using an HD Hokuto Denko Ltd. HA-301 potentiostat–galvanostat in 5 × 10^{-4} M (*n*-

(1) Plumb, C. A.; Carroll, P. J.; Sneddon, L. G. *Organometallics*, preceding paper in this issue.

(2) A commo nickela bis(tricarbaborane) analogue of nickelocene, commo-*Ni*-(1-Ni-2,3-Me_2-4,6-Et_2-2,3,5-C_3B_2H)$_2$, based on the tricarbon heterocyclic $R_4C_3B_2H$ system, has previously been reported by Siebert; see: (a) Kuhlmann, T.; Pritzkow, H.; Zenneck, U.; Siebert, W. *Angew. Chem., Int. Ed. Engl.* **1984**, *23*, 965–966. (b) Zwecker, J.; Pritzkow, H.; Zenneck, U.; Siebert, W. *Angew. Chem., Int. Ed. Engl.* **1986**, *25*, 1099–1100. (c) Zwecker, J.; Kuhlmann, T.; Pritzkow, H.; Siebert, W.; Zenneck, U. *Organometallics* **1988**, *7*, 2316–2324. (d) Siebert, W.; Schafer, V.; Brodt, G.; Fessenbecker, A.; Pritzkow, H. *Abstracts of Papers*, 200th National Meeting of the American Chemical Society, Washington, DC, Aug 1990; American Chemical Society: Washington, DC, 1990; INOR 381.

(3) Shriver, D. F.; Drezdzon, M. A. *Manipulation of Air Sensitive Compounds*, 2nd ed.; Wiley: New York, 1986.

(4) Kang, S. O.; Furst, G. T.; Sneddon, L. G. *Inorg. Chem.* **1989**, *28*, 2339–2347.

(5) Kovaic, P.; Brace, N. O. *Inorg. Synth.* **1960**, *6*, 172.

(6) Kang, S. O.; Carroll, P. J.; Sneddon, L. G. *Organometallics* **1988**, *7*, 772–776.

(7) (a) Evans, D. F. *J. Chem. Soc.* **1959**, 2003–2005. (b) Crawford, T. H.; Swanson, J. *J. Chem. Educ.* **1971**, *48*, 382–386. (c) Carlin, R. L. *J. Chem. Educ.* **1966**, *43*, 521–525.

0276-7333/92/2311-1672$03.00/0

Table I. NMR Data[a]

compd	nucleus	δ (mult, J (Hz))
commo-Fe-(1-Fe-2-CH_3-2,3,5-$C_3B_7H_9$)$_2$ (6)	^{11}B[b]	5.9 (d, 164), −0.5 (d, 155), −1.4 (d, overlapped), −2.0 (d, 164), −20.1 (d, 177), −21.4 (d, 183), −32.3 (d, 163)
	^{1}H[c]	6.56 (s, C3H), 2.01 (s, CH_3), 1.55 (s, C5H)
commo-1-*Fe*-(5-CH_3-2,3,5-$C_3B_7H_9$)$_2$ (7)	^{11}B (27 °C)	16.6, −1.5, −8.9, −15.5, −19.4, −23.4, −37.2
	^{11}B (90 °C)	26.5, −7.1, −12.5, −13.4, −13.9, −19.5, −35.4, −41.6
	^{1}H[c] (90 °C)	9.53 (br s, CH_3), 7.85 (q, 160, BH), 3.18 (q, 154, BH), 1.32 (q, ∼150, BH), ∼0.13 (q, 145, BH), −0.60 (s, CH), −1.73 (q, 175, BH), −4.93 (q, 146, BH), −6.10 (s, CH)
	^{1}H[c] (−50 °C)	4.58 (br s, CH), 3.84 (br s, CH), 1.95 (s, CH_3)
commo-Fe-(1-Fe-5-CH_3-2,3,5-$C_3B_7H_9$)(4-CH_3-2,3,4-$C_3B_7H_9$) (8)	^{11}B[c]	7.9 (d, 161), −1.8 (d, 188), −3.4 (d, 155, 2 B), −19.0 (d, 142, 2 B), −26.6 (d, 163)
	^{1}H[c]	6.05 (s, C3(2)H), 5.41 (s, C2(3)H), 0.93 (s, CH_3)
commo-1-*Fe*-(10-CH_3-2,3,10-$C_3B_7H_9$)$_2$ (9)	^{11}B[b]	3.72 (d, 205), −11.7 (d, 155), −14.1 (d, 166), −24.5 (d, 159)
	^{1}H[c]	5.79 (s, C2(3)H), 5.55 (s, C3(2)H), 1.12 (s, CH_3)

[a] In C_6D_6. [b] 160 MHz. [c] 500 MHz.

butyl)$_4$NPF$_6$ electrolyte–acetonitrile solutions referenced to SCE. Preparative thin-layer chromatography was conducted on 0.5 mm (20 × 20 cm) silica gel F-254 plates (Merck 5744). Analytical thin-layer chromatography was performed on 0.25 mm (5 × 10 cm) silica gel F-254 plates (Merck). Silica gel (230–400 mesh, Merck) was used for flash column chromatography. Elemental analyses were obtained from Galbraith Laboratories, Inc., Knoxville, TN. The yields of all metallatricarbaborane products are calculated on the basis of starting metal reagent.

Ferratricarbaborane Complexes 6–8. A 2.47-mmol (0.313-g) sample of $FeCl_2$ was loaded into a 100-mL three-neck round-bottom flask equipped with a stirbar, septum, and vacuum stopcock. The flask was evacuated and 20 mL of THF vacuum-distilled into the flask. The mixture was warmed to room temperature and a 27.5-mL aliquot of a 0.18 M Na$^+$(5,6,9-$CH_3C_3B_7H_9$)$^-$/THF solution added dropwise via syringe. The solution turned pale green immediately and then gradually brown-red as the solution was stirred for 16 h. The reaction mixture was opened to the air and filtered through a glass frit and the resultant red-orange solution evaporated to dryness. The crude product was then dissolved in CH_2Cl_2 and the solution quickly eluted through a 6-in. plug of silica gel with hexane. The filtrate was evaporated to dryness and dissolved in a minimum of hot hexane and the solution placed in a −5 °C refrigerator to crystallize overnight. Filtration of the resulting precipitate yielded brown-red crystals of *commo-Fe*-(1-Fe-2-CH_3-2,3,5-$C_3B_7H_9$)$_2$ (6). The process was then repeated with the remaining hexane-soluble material until no further crystallization was observed (0.388 g, 1.16 mmol, 47% yield). Separation of the material in the filtrate (0.329 g, 1.05 mmol) by preparative TLC (7:3 hexane–CH_2Cl_2) produced two bands. The reddish pink first band (R_f 0.72) yielded 62 mg (0.19 mmol) of *commo-Fe*-(1-Fe-5-CH_3-2,3,5-$C_3B_7H_9$)$_2$ (7), while the second reddish-brown band (R_f 0.69) produced 152 mg (0.46 mmol) of *commo-Fe*-(1-Fe-5-CH_3-2,3,5-$C_3B_7H_9$)(1-Fe-4-CH_3-2,3,4-$C_3B_7H_9$) (8). Overall the ferratricarbaborane yield was 74% and the ratio of isomers was 6.3:1:2.4 (6:7:8). For 6: brown-red; mp 189 °C; IR (KBr, cm^{-1}) 3058 (vw), 3035 (w), 2998 (vw), 2976 (vw), 2608 (sh, s), 2558 (s), 2360 (vw), 2355 (vw), 1440 (s), 1382 (w), 1372 (vw), 1275 (w), 1128 (m), 1092 (m), 1044 (s), 958 (s), 932 (vw), 910 (w), 905 (vw), 894 (vw), 868 (m), 836 (w), 822 (vw), 798 (w), 760 (w), 724 (s), 695 (w), 647 (w), 615 (vw), 600 (vw), 502 (m), 335 (w); UV–vis (λ, nm (ε, L cm^{-1} mol^{-1}), in CH_2Cl_2) 236 (5531), 294 (4391, sh), 420 (572). Anal. Calcd for $C_8H_{24}B_{14}Fe$: C, 29.34; H, 7.38. Found: C, 29.83; H, 7.42. Exact mass measurement for $^{12}C_8{}^1H_{24}{}^{11}B_{14}{}^{56}Fe$: calcd, 330.2530; found, 330.2567. For 7: pink-red; mp 177 °C; IR (KBr, cm^{-1}) 2950 (w), 2920 (w), 2608 (sh), 2560 (s), 1318 (w), 1258 (w), 1182 (sh), 1175 (vw), 1112 (w), 1110 (w), 1086 (w), 1035 (m), 936 (m), 876 (w), 858 (sh), 720 (m); UV–vis (λ, nm (ε, L cm^{-1} mol^{-1}), in CH_2Cl_2) 234 (5538), 288 (4094, sh), 502 (284). Anal. Calcd for $C_8H_{24}B_{14}Fe$: C, 29.34; H, 7.38. Found: C, 29.16; H, 7.50. Exact mass measurement for $^{12}C_8{}^1H_{24}{}^{11}B_{14}{}^{56}Fe$: calcd, 330.2530; found, 330.2568. For 8: red-brown; mp 113 °C; IR (KBr, cm^{-1}) 2920 (w), 2660 (s), 2640 (sh), 1380 (w), 1260 (w), 1175 (w), 1100 (w), 1088 (w), 1040 (w), 1030 (sh), 948 (w), 928 (w), 913 (w), 860 (w), 835 (w), 722 (w); UV–vis (λ, nm (ε, L cm^{-1} mol^{-1}), in CH_2Cl_2) 230 (5618), 284 (4981, sh), 330 (1631). Anal. Calcd for $C_8H_{24}B_{14}Fe$: C, 29.34; H, 7.38. Found: C, 29.40; H, 7.52. Exact mass measurement for $^{12}C_8{}^1H_{24}{}^{11}B_{14}{}^{56}Fe$: calcd, 330.2530; found, 330.2511.

Thermal Rearrangement Reactions. Synthesis of 9. Rearrangement reactions were carried out in 5-mm Pyrex tubes in which ∼10-mg samples of 6 were sealed off in vacuo and then placed into a temperature-stabilized silicone oil bath. After they were heated for 4 h, the samples were cooled to room temperature and examined by ^{11}B NMR spectroscopy.

Below 190 °C no reaction was observed. At 230 °C, resonances due to 6 were observed to be entirely replaced by peaks matching those of 7 (∼15%) and 8 (∼85%). At 250 °C, 90% conversion to *commo-Fe*-(1-Fe-10-CH_3-2,3,10-$C_3B_7H_9$)$_2$ (9) was observed. An 80-mg sample of 6 heated at 250 °C overnight gave 73 mg (0.22 mmol, 91%) of 9 (R_f 0.86, 7:3 hexane–CH_2Cl_2) and 6.5 mg of a red substance (R_f 0.76) which, according to mass spectral and TLC analysis, appeared to be a mixture of two new isomers. These two new isomers were not produced in sufficient quantities to allow further characterization. Isomer 7 could not be obtained alone at any temperature. After pure samples of 7 and 8 were heated, in separate sealed tubes, for 45 min at 240 °C, identical mixtures of 7 (∼10%) and 8 (∼90%) were obtained. For 9: green; mp 187.5 °C; IR (KBr, cm^{-1}) 2922 (w), 2585 (sh), 2560 (s), 1450 (w), 1260 (w), 1184 (w), 1122 (m), 1095 (w), 1054 (w), 1044 (sh), 1038 (w), 976 (sh), 900 (w), 890 (sh), 876 (sh), 840 (w), 820 (w), 786 (w), 750 (sh), 730 (w); UV–vis (λ, nm (ε, L cm^{-1} mol^{-1}), in CH_2Cl_2) 222 (4500, sh), 262 (6167), 316 (1414). Anal. Calcd for $C_8H_{24}B_{14}Fe$: C, 29.34; H, 7.38. Found: C, 27.98; H, 7.17. Exact mass measurement for $^{12}C_8{}^1H_{24}{}^{11}B_{14}{}^{56}Fe$: calcd, 330.2530; found, 330.2480.

Cobaltatricarbaborane Complexes 10 and 11. A 0.50-mmol (0.065-g) sample of $CoCl_2$ was loaded into a 50-mL three-neck round-bottom flask equipped with a stirbar, septum, and vacuum stopcock. The flask was then evacuated and 20 mL of THF added by vacuum distillation. The mixture was warmed to room temperature and a 5-mL sample of 0.25 M Na$^+$(5,6,9-$CH_3C_3B_7H_9$)$^-$ in THF added dropwise by syringe. The solution immediately turned from deep blue to dark green. The reaction was continued for 16 h; then the mixture was opened to the air and filtered through a 1-in. plug of silica gel. The dark green filtrate was evaporated to dryness, the residue was redissolved in CH_2Cl_2 and this solution was separated into three bands on TLC plates (7:3 hexane–CH_2Cl_2). A light green band (R_f 0.88) yielded 43 mg (0.13 mmol, 17%) of *commo-Co*-(1-Co-2-CH_3-2,3,5-$C_3B_7H_9$)(1-Co-5-CH_3-2,3,5-$C_3B_7H_9$) (10). For 10: light green; mp 107–108 °C; IR (KBr, cm^{-1}) 3048 (vw), 2920 (vw), 2570 (sh), 2550 (s), 1438 (m), 1378 (m), 1278 (sh), 1260 (w), 1288 (w), 1130 (m), 1095 (sh), 1080 (m), 1048 (vw), 1038 (m), 1020 (sh), 958 (m), 920 (m), 870 (w), 820 (w), 728 (m), 710 (sh), 675 (vw), 544 (vw), 460 (vw), 415 (vw); UV–vis (λ, nm (ε, L cm^{-1} mol^{-1}), in CH_2Cl_2) 234 (4590), 284 (4188, sh), 362 (2055). Anal. Calcd for $C_8H_{24}B_{14}Co$: C, 29.07; H, 7.31. Found: C, 29.91; H, 7.41. Exact mass measurement for $^{12}C_8{}^1H_{24}{}^{11}B_{14}{}^{59}Co$: calcd, 333.2513; found, 333.2557. A dark green band (R_f 0.70) yielded 95 mg (0.29 mmol, 38%) of *commo-Co*-(1-Co-2-CH_3-2,3,5-$C_3B_7H_9$)$_2$ (11). For 11: dark green; mp 149.5 °C; μ = 1.69 μ_B; IR (KBr, cm^{-1}) 3038 (vw), 2910 (vw), 2608 (sh), 2580 (sh), 2560 (s), 1438 (m), 1380 (m), 1276 (m), 1184 (w), 1132 (m), 1095 (m), 1060 (w), 1056 (m), 1022 (m), 986 (w), 965 (m), 932 (m), 920 (m), 888 (m), 866 (w), 822 (w), 818 (w), 796 (w), 754 (w),

Table II. Data Collection and Structure Refinement Information

	6	7	8
space group	*Pnna*	*P*$\bar{1}$	$P2_1/n$
a, Å	13.572 (2)	7.475 (2)	10.394 (1)
b, Å	11.986 (1)	9.524 (1)	14.013 (2)
c, Å	10.276 (1)	12.769 (1)	12.597 (2)
α, deg		96.96 (1)	
β, deg		94.91 (1)	108.87 (1)
γ, deg		106.48 (1)	
V, Å^3	1671.7 (5)	858.3 (5)	1736.2 (8)
Z	4	2	4
D_{calcd}, g cm^{-3}	1.301	1.267	1.253
F(000)	672	336	672
mol formula	$FeC_8H_{24}B_{14}$	$FeC_8H_{24}B_{14}$	$FeC_8H_{24}B_{14}$
mol wt	327.48	327.48	327.48
λ, Å	Mo Kα, 0.710 73	Mo Kα, 0.710 73	Mo Kα, 0.710 73
μ, cm^{-1}	8.8	8.6	8.5
tranmissn (min, max)	93.1, 99.9	92.5, 99.9	98.8, 100.0
θ range, deg	2–27.5	2–27.5	2–27.5
scan mode	ω–2θ	ω–2θ	ω–2θ
$\pm h,\pm k,\pm l$ collected	17,15,13	9,±12,±16	±13,–18,16
no. of measd intens	2203	4244	4338
no. of unique intens	1920	3944	3987
no. of $F_o^2 > 3\sigma(F_o^2)$	1414	3567	2315
no. of variables	105	208	208
R	0.037	0.032	0.045
R_w	0.060	0.052	0.055
GOF	1.94	1.82	1.38

	9	10	11
space group	*P*$\bar{1}$	*C*2/*c*	*P*$\bar{1}$
a, Å	6.935 (3)	20.788 (4)	7.754 (4)
b, Å	9.743 (6)	15.115 (3)	17.649 (5)
c, Å	12.861 (3)	12.626 (2)	6.721 (1)
α, deg	92.58 (3)		90.99 (2)
β, deg	82.96 (3)	118.28 (2)	107.53 (3)
γ, deg	105.51 (5)		102.20 (3)
V, Å^3	831 (1)	3494 (3)	854 (1)
Z	2	8	2
F(000)	336	1352	338
D_{calcd}, g cm^{-3}	1.309	1.257	1.285
mol formula	$FeC_8H_{24}B_{14}$	$CoC_8H_{24}B_{14}$	$CoC_8H_{24}B_{14}$
mol wt	327.48	330.57	330.57
λ, Å	Mo Kα, 0.710 73	Mo Kα, 0.710 73	Mo Kα, 0.710 73
μ, cm^{-1}	8.9	9.6	9.8
tranmissn (min, max)	71.4, 99.7	89.3, 99.9	93.6, 99.9
θ range, deg	2–27.5	2–27.5	2–27.5
scan mode	ω–2θ	ω–2θ	ω–2θ
$\pm h,\pm k,\pm l$ collected	9,±12,±16	±27,19,16	10,±22,±8
no. of measd intens	4109	4344	4199
no. of unique intens	3790	4008	3907
no. of $F_o^2 > 3\sigma(F_o^2)$	2880	3034	3298
no. of variables	208	208	208
R	0.078	0.034	0.034
R_w	0.097	0.049	0.051
GOF	2.57	1.48	1.61

730 (sh), 716 (w), 704 (w), 680 (w), 600 (vw), 554 (vw), 520 (vw), 460 (vw); UV–vis (λ, nm (ϵ, L cm^{-1} mol^{-1}), in CH_2Cl_2) 230 (4697), 290 (4079, sh), 364 (1793). Anal. Calcd for $C_8H_{24}B_{14}Co$: C, 29.07; H, 7.31. Found: C, 29.22; H, 7.55. Exact mass measurement for $^{12}C_8{}^1H_{24}{}^{11}B_{14}{}^{59}Co$: calcd, 333.2513; found, 333.2523. A green-brown band (R_f 0.15) produced 67 mg of material, but attempts to characterize this material were unsuccessful.

The oxidation of isomer **11** from Co^{II} to Co^{III} was attempted using several oxidizing agents, including $Cp_2Fe^+BF_4^-$, aqueous HCl, H_2O_2 in THF, and acidic Pb_2O_2. However, according to TLC and/or NMR analyses, no 11^+ was formed.

Table III. Refined Positional Parameters for 6

atom	*x*	*y*	*z*	B_{eq},[a] Å^2
Fe1	0.12394 (3)	0.2500	0.2500	2.183 (8)
C2	0.0271 (2)	0.3208 (2)	0.3744 (2)	2.64 (4)
C2m	–0.0631 (2)	0.3858 (2)	0.3304 (3)	3.34 (5)
C3	0.2128 (2)	0.1597 (2)	0.3563 (3)	3.16 (5)
B4	0.1300 (2)	0.3759 (2)	0.4124 (3)	2.97 (6)
C5	0.0178 (2)	0.2096 (2)	0.4351 (2)	3.00 (5)
B6	0.1135 (2)	0.1124 (3)	0.4107 (3)	3.28 (6)
B7	0.2378 (2)	0.2808 (3)	0.4082 (3)	3.22 (6)
B8	0.0481 (2)	0.3189 (3)	0.5384 (3)	3.46 (6)
B9	0.2132 (2)	0.1666 (3)	0.5172 (3)	3.80 (7)
B10	0.1738 (2)	0.3023 (3)	0.5589 (3)	3.61 (6)
B11	0.0890 (2)	0.1832 (3)	0.5661 (3)	3.82 (7)

[a] $B_{eq} = {}^4/_3[\beta_{11}a^2 + \beta_{22}b^2 + \beta_{33}c^2 + \beta_{12}ab(\cos\gamma) + \beta_{13}ac(\cos\beta) + \beta_{23}bc(\cos\alpha)]$.

Crystallographic Data for 6–11. Single crystals were grown by slow evaporation in air of methylene chloride–hexane solutions. Suitably sized crystals were mounted and transferred to the diffractometer. Refined cell dimensions and their standard deviations were obtained from least-squares refinement of 25 accurately centered reflections.

Collection and Reduction of the Data. Diffraction data were collected at 295 K on an Enraf-Nonius four-circle CAD-4 diffractometer employing Mo Kα radiation from a highly oriented graphite-crystal monochromator. The intensities of three standard reflections measured at regular intervals showed no systematic change during data collection. The raw intensities were corrected for Lorentz and polarization effects by using the Enraf-Nonius program BEGIN.

Solution and Refinement of the Structure. All calculations were performed on a VAX 11/750 computer using the Enraf-Nonius structure package. The full-matrix least-squares refinement was phased on *F*, and the function minimized was $\sum w(|F_o| - |F_c|)^2$. The weights (w) were taken as $4F_o^2/(\sigma(F_o^2))^2$, where $|F_o|$ and $|F_c|$ are the observed and calculated structure factor amplitudes. The neutral-atom scattering factors and complex anomalous dispersion corrections are those stored in the SDP package. Agreement factors are defined as $R = \sum||F_o| - |F_c||/\sum|F_o|$ and $R_w = (\sum(|F_o| - |F_c|)^2/\sum|F_o|^2)^{1/2}$.

Three-dimensional Patterson syntheses gave the coordinates of the metal atoms in all compounds. Subsequent Fourier maps led to the locations of all other non-hydrogen atoms. Anisotropic refinements followed by difference Fourier syntheses resulted in the location of all cage hydrogens. The positions of the remaining hydrogens were then calculated. Hydrogen atoms were not refined but included as constant contributions to the structure factors. The final refinement included either numerical or empirical absorption corrections along with anisotropic thermal parameters for non-hydrogen atoms and fixed isotropic thermal parameters for the hydrogen atoms (6 Å^2). Final difference Fouriers were featureless. Crystal and refinement data are given in Table II. Final positional parameters are given in Tables III–VIII. Selected intramolecular bond distances are presented in the figure captions.

Results and Discussion

The reaction of $FeCl_2$ and 2 equiv of $Na^+(6\text{-}CH_3\text{-}5,6,9\text{-}C_3B_7H_9)^-$ yielded three different isomeric *commo*-ferratricarbaborane products, the compositions of which were initially established by both elemental analyses and exact mass determinations:

$$2(Na^+6\text{-}CH_3\text{-}5,6,9\text{-}C_3B_7H_9)^- \xrightarrow[-2NaCl]{FeCl_2} \underset{\mathbf{6}}{\textit{commo}\text{-}Fe\text{-}(1\text{-}Fe\text{-}2\text{-}CH_3\text{-}2,3,5\text{-}C_3B_7H_9)_2} + \underset{\mathbf{7}}{\textit{commo}\text{-}Fe\text{-}(1\text{-}Fe\text{-}5\text{-}CH_3\text{-}2,3,5\text{-}C_3B_7H_9)_2} + \underset{\mathbf{8}}{\textit{commo}\text{-}Fe\text{-}(1\text{-}Fe\text{-}5\text{-}CH_3\text{-}2,3,5\text{-}C_3B_7H_9)\text{-}(1\text{-}Fe\text{-}4\text{-}CH_3\text{-}2,3,4\text{-}C_3B_7H_9)} \quad (1)$$

Table IV. Refined Positional Parameters for 7

atom	x	y	z	B_{eq},[a] Å^2
Fe1	0.76747 (3)	0.99000 (2)	0.75593 (2)	2.156 (4)
C2	0.7876 (3)	0.7940 (2)	0.6987 (2)	2.97 (4)
C3	0.5187 (3)	0.9522 (2)	0.8027 (2)	3.21 (4)
B4	0.7743 (3)	0.7820 (2)	0.8205 (2)	3.19 (4)
C5	0.6017 (3)	0.7608 (2)	0.6357 (2)	3.23 (4)
C5m	0.5860 (4)	0.7302 (3)	0.5158 (2)	5.23 (6)
B6	0.4587 (3)	0.8646 (2)	0.6860 (2)	3.36 (4)
B7	0.6110 (3)	0.8697 (3)	0.8809 (2)	3.39 (5)
B8	0.6358 (4)	0.6335 (2)	0.7178 (2)	3.54 (5)
B9	0.3821 (3)	0.7837 (3)	0.8048 (2)	3.81 (5)
B10	0.5315 (4)	0.6757 (3)	0.8281 (2)	3.60 (5)
B11	0.4206 (4)	0.6693 (3)	0.6947 (2)	3.55 (5)
C2a	0.9207 (3)	1.1295 (2)	0.8801 (1)	2.97 (4)
C3a	0.8159 (3)	1.0952 (2)	0.6343 (1)	3.11 (4)
B4a	1.0718 (3)	1.0929 (3)	0.8113 (2)	3.37 (4)
C5a	0.8513 (3)	1.2491 (2)	0.8458 (2)	3.14 (4)
C5ma	0.7440 (4)	1.3240 (3)	0.9176 (2)	5.00 (5)
B6a	0.7679 (3)	1.2191 (2)	0.7100 (2)	3.11 (4)
B7a	1.0174 (3)	1.0798 (3)	0.6667 (2)	3.50 (4)
B8a	1.0967 (4)	1.2817 (3)	0.8689 (2)	3.79 (5)
B9a	0.9818 (4)	1.2537 (3)	0.6428 (2)	3.82 (5)
B10a	1.1572 (3)	1.2521 (3)	0.7420 (2)	3.87 (5)
B11a	0.9904 (4)	1.3539 (2)	0.7699 (2)	3.61 (5)

[a] See footnote *a* in Table III.

Table V. Refined Positional Parameters for 8

atom	x	y	z	B_{eq},[a] Å^2
C1	0.8041 (1)	0.3119 (3)	1.1073 (1)	3.91 (3)
Fe1	0.04356 (5)	0.10842 (4)	0.25948 (4)	2.911 (9)
C2	0.1161 (4)	0.0815 (3)	0.1347 (3)	4.13 (9)
C3	0.2027 (4)	0.1241 (3)	0.3915 (3)	4.6 (1)
B4	0.1590 (5)	−0.0080 (4)	0.2126 (4)	4.6 (1)
C5	0.2108 (4)	0.1628 (3)	0.1710 (3)	4.6 (1)
C5m	0.2039 (6)	0.2435 (4)	0.0906 (4)	8.2 (1)
B6	0.2444 (5)	0.1952 (4)	0.3125 (4)	5.0 (1)
B7	0.2176 (6)	0.0159 (4)	0.3647 (4)	5.2 (1)
B8	0.2772 (5)	0.0505 (4)	0.1561 (4)	5.2 (1)
B9	0.3557 (6)	0.0992 (5)	0.3914 (5)	6.3 (2)
B10	0.3374 (5)	0.0079 (4)	0.2913 (5)	5.7 (1)
B11	0.3629 (5)	0.1310 (5)	0.2600 (5)	6.3 (1)
C2a	−0.0742 (4)	0.2170 (3)	0.1860 (3)	3.60 (8)
C3a	−0.0654 (4)	0.0287 (3)	0.3253 (3)	4.5 (1)
C4a	−0.0936 (4)	0.2275 (3)	0.2971 (3)	3.80 (9)
C4ma	−0.0463 (4)	0.3186 (3)	0.3627 (4)	5.1 (1)
B5a	−0.1591 (5)	0.1321 (4)	0.1161 (4)	4.4 (1)
B6a	−0.1536 (5)	0.0218 (4)	0.1958 (4)	4.7 (1)
B7a	−0.0826 (5)	0.1257 (4)	0.3800 (3)	4.1 (1)
B8a	−0.2393 (5)	0.2227 (4)	0.1725 (4)	5.0 (1)
B9a	−0.2279 (5)	0.0539 (5)	0.3044 (4)	5.5 (1)
B10a	−0.2420 (5)	0.1771 (5)	0.3003 (4)	4.9 (1)
B11a	−0.2913 (5)	0.1054 (5)	0.1720 (4)	5.3 (1)

[a] See footnote *a* in Table III.

Table VI. Refined Positional Parameters for 9

atom	x	y	z	B_{eq},[a] Å^2
Fe1	0.2354 (1)	0.50556 (7)	0.24555 (5)	2.14 (1)
C2	0.1720 (8)	0.4625 (5)	0.0980 (4)	2.7 (1)
C3	0.1464 (8)	0.3245 (5)	0.3255 (4)	2.9 (1)
C10	0.1643 (8)	0.1998 (6)	0.1410 (4)	3.2 (1)
C10m	0.218 (1)	0.0719 (7)	0.0880 (5)	4.7 (2)
B4	0.3179 (9)	0.3693 (6)	0.1098 (5)	2.8 (1)
B5	−0.0422 (9)	0.4037 (7)	0.1566 (5)	3.1 (1)
B6	−0.061 (1)	0.3212 (7)	0.2862 (5)	3.3 (1)
B7	0.3053 (9)	0.2933 (6)	0.2388 (5)	3.0 (1)
B8	0.071 (1)	0.2972 (7)	0.0633 (5)	3.3 (1)
B9	0.053 (1)	0.1754 (7)	0.2648 (5)	3.4 (1)
B11	−0.086 (1)	0.2152 (7)	0.1713 (5)	3.4 (1)
C2a	0.1128 (8)	0.6045 (6)	0.3626 (4)	2.9 (1)
C3a	0.5025 (7)	0.6318 (5)	0.1936 (4)	2.6 (1)
C10a	0.4793 (8)	0.7582 (6)	0.3770 (4)	3.2 (1)
C10ma	0.617 (1)	0.8349 (7)	0.4577 (5)	4.6 (1)
B4a	0.3106 (9)	0.5975 (7)	0.4068 (4)	3.0 (1)
B5a	0.1459 (9)	0.7163 (7)	0.2749 (5)	3.1 (1)
B6a	0.3707 (9)	0.7354 (6)	0.1787 (5)	2.8 (1)
B7a	0.5296 (8)	0.6096 (6)	0.3097 (5)	2.7 (1)
B8a	0.237 (1)	0.7633 (7)	0.4028 (5)	3.5 (1)
B9a	0.5858 (9)	0.7858 (7)	0.2521 (5)	3.2 (1)
B11a	0.376 (1)	0.8490 (7)	0.2905 (5)	3.3 (1)

[a] See footnote *a* in Table III.

Table VII. Refined Positional Parameters for 10

atom	x	y	z	B_{eq},[a] Å^2
Co1	0.24148 (1)	0.11694 (2)	0.22100 (2)	2.739 (6)
C2	0.3434 (1)	0.1741 (2)	0.3212 (2)	3.99 (6)
C2m	0.3560 (2)	0.2480 (2)	0.4104 (3)	6.84 (9)
C3	0.2661 (1)	0.0122 (2)	0.1556 (2)	3.99 (5)
C5	0.3793 (1)	0.0894 (2)	0.3673 (2)	4.52 (6)
B4	0.3238 (1)	0.1857 (2)	0.1841 (2)	3.82 (6)
B6	0.3309 (2)	−0.0030 (2)	0.2874 (3)	4.61 (7)
B7	0.2809 (1)	0.0862 (2)	0.0853 (2)	3.80 (6)
B8	0.4144 (2)	0.1521 (3)	0.2941 (3)	4.77 (7)
B9	0.3439 (2)	−0.0038 (2)	0.1534 (3)	4.58 (7)
B10	0.3764 (1)	0.1033 (2)	0.1530 (3)	4.35 (7)
B11	0.4134 (2)	0.0360 (3)	0.2887 (3)	4.92 (8)
C2a	0.1675 (1)	0.2083 (2)	0.1152 (2)	3.37 (5)
C3a	0.1841 (1)	0.0525 (2)	0.2826 (2)	4.94 (6)
C5a	0.1064 (1)	0.1469 (2)	0.0584 (2)	3.77 (5)
C5ma	0.0700 (2)	0.1317 (2)	−0.0764 (3)	5.96 (9)
B4a	0.1848 (2)	0.2364 (2)	0.2460 (3)	4.17 (7)
B6a	0.1215 (2)	0.0500 (2)	0.1464 (3)	4.88 (8)
B7a	0.1916 (2)	0.1421 (2)	0.3477 (2)	5.13 (7)
B8a	0.0925 (1)	0.2389 (2)	0.1252 (3)	3.87 (6)
B9a	0.1056 (2)	0.0860 (3)	0.2707 (3)	6.48 (8)
B10a	0.1080 (2)	0.2023 (3)	0.2651 (3)	5.12 (7)
B11a	0.0561 (2)	0.1359 (2)	0.1292 (3)	4.85 (7)

[a] See footnote *a* in Table III.

Given the similarity of these isomeric systems, correct structural assignments would not have been possible on the basis of spectral evidence alone; therefore, single-crystal X-ray studies of each isomer were undertaken and the results of these determinations are shown in the ORTEP drawings in Figures 1–3.

As can be seen in Figures 1–3, the complexes can be considered ferrocene analogues in which a formal Fe^{2+} ion is sandwiched between two tricarbon carborane ligands. Like a (η-C_5H_5)Fe group, a ($CH_3C_3B_7H_9$)Fe fragment can be considered to donate one skeletal electron to a second $CH_3C_3B_7H_9$ cage. Therefore, each Fe(CH_3)$C_3B_7H_9$ cage would be an 11-vertex 24-skeletal-electron system that should adopt a closo-octadecahedral geometry. The ferra bis(tricarbaborane) complexes could therefore also be described as two closo-octadecahedral cages sharing a common vertex (iron).

That several isomers are produced in both the ferratricarbaborane and the cobaltatricarbaborane reactions, discussed below, is the result of several factors. First, the 6-CH_3-5,6,9-$C_3B_7H_9^-$ anion exists as a racemic mixture:

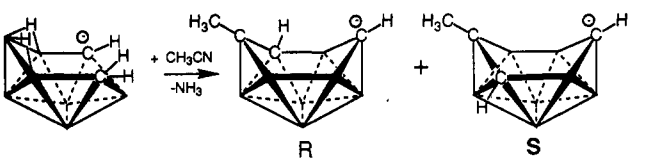

When a bis-cage complex is formed from this racemic anion mixture, two possible isomeric complexes can result: (1) a complex containing two anion cages of the same enantiomeric type (*SS* or *RR*; **6**, **7**, and **9**–**11**) or (2) a complex containing two different enantiomeric forms of the anion (*RS*; **8**).

Second, as was observed in the monocage ferratricarbaborane complexes discussed in the preceding paper,[1] cage rearrangements can produce additional isomers. Rearrangements involving the carbon skeleton or

Table VIII. Refined Positional Parameters for 11

atom	x	y	z	B_{eq},[a] Å^2
Co1	0.04501 (4)	0.24881 (2)	0.16557 (4)	2.080 (5)
C2	0.0498 (3)	0.3618 (1)	0.2582 (3)	2.45 (4)
C2m	−0.0812 (3)	0.3761 (1)	0.3754 (4)	3.35 (5)
C3	0.2836 (3)	0.2687 (1)	0.1002 (4)	3.00 (5)
C5	0.2510 (3)	0.3828 (1)	0.3742 (4)	3.02 (5)
B4	0.0141 (4)	0.3598 (2)	0.0112 (4)	2.74 (5)
B6	0.3812 (4)	0.3246 (2)	0.3091 (5)	3.33 (6)
B7	0.1626 (4)	0.3059 (2)	−0.0855 (4)	2.90 (5)
B8	0.1711 (4)	0.4424 (2)	0.1839 (5)	3.28 (6)
B9	0.3986 (4)	0.3542 (2)	0.0529 (5)	3.43 (6)
B10	0.2284 (4)	0.4094 (2)	−0.0293 (4)	3.19 (6)
B11	0.3920 (4)	0.4235 (2)	0.2364 (5)	3.48 (6)
C2a	0.0958 (3)	0.1486 (1)	0.3042 (4)	2.66 (4)
C2ma	0.2905 (4)	0.1496 (2)	0.4440 (5)	3.92 (6)
C3a	−0.2298 (3)	0.2196 (1)	0.0776 (4)	2.66 (4)
C5a	−0.0521 (3)	0.1388 (1)	0.4044 (4)	2.85 (5)
B4a	0.0122 (4)	0.1229 (2)	0.0595 (4)	2.82 (5)
B6a	−0.2237 (4)	0.1883 (2)	0.2980 (4)	2.91 (5)
B7a	−0.1944 (4)	0.1628 (2)	−0.0796 (4)	2.87 (5)
B8a	−0.0567 (4)	0.0604 (2)	0.2450 (5)	3.18 (6)
B9a	−0.3629 (4)	0.1311 (2)	0.0505 (5)	3.21 (6)
B10a	−0.2245 (4)	0.0684 (2)	0.0098 (4)	3.23 (6)
B11a	−0.2605 (4)	0.0833 (2)	0.2642 (5)	3.29 (6)

[a] See footnote *a* in Table III.

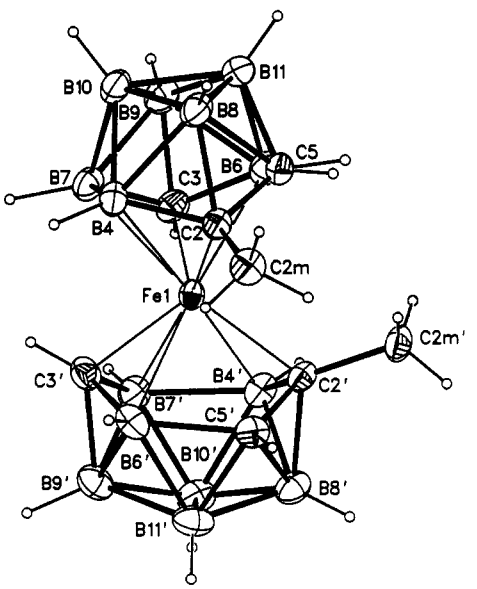

Figure 1. ORTEP drawing of the molecular structure of *commo-Fe*-(1-Fe-2-CH_3-2,3,5-$C_3B_7H_9$)$_2$ (**6**). Selected bond distances (Å): Fe–C2, 2.021 (2); Fe–C3, 1.955 (3); Fe–B4, 2.251 (3); Fe–C5, 2.435 (3); Fe–B6, 2.338 (3); Fe–B7, 2.273 (3); C2–C5, 1.478 (4); C2–B4, 1.593 (4); B4–B7, 1.854 (4); C3–B7, 1.583 (4); C3–B6, 1.565 (4).

the exopolyhedral methyl group are possible. For the commo ferra and cobalta bis(tricarbaborane) complexes, cage isomers were produced with the methyl carbon unit at the 2-vertex (**6** and **10**), the 4(5)-vertex (**7**, **8**, **10**, **11**), and the 10-vertex positions (**9**).

Additional isomers are also possible due to differences in the orientation of the two cages relative to each other. Indeed, the structures in the figures show that the cages may be oriented in at least two different configurations, with the C4 (C5) or C10 carbons on either the same ("cis") (**6**, **8**, **9**, and **11**) or opposite ("trans") (**7** and **10**) of the molecule.

For the commo ferra bis(tricarbaboranes), the major product **6** (Figure 1) was the expected product with the methyl group substituted at the C2 position, as in the 6-CH_3-5,6,9-$C_3B_7H_9^-$ anion, and is composed of only one type of anion enantiomer (equal mixture of *RR* and *SS*)

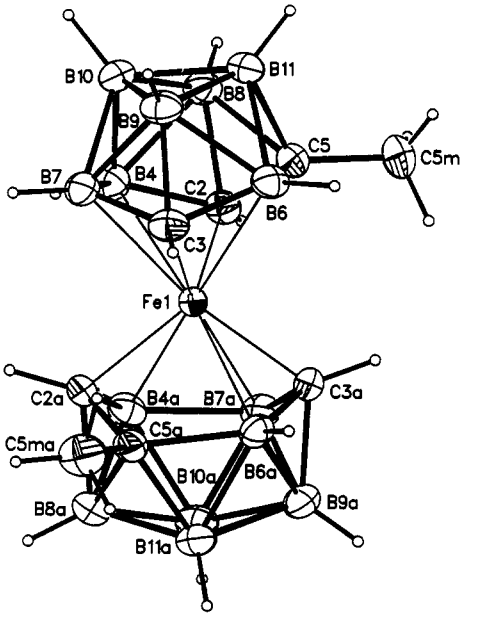

Figure 2. ORTEP drawing of the molecular structure of *commo-Fe*-(1-Fe-5-CH_3-2,3,5-$C_3B_7H_9$)$_2$ (**7**). Selected bond distances (Å): Fe–C2, 1.972 (2); Fe–C3, 1.951 (2); Fe–B4, 2.247 (2); Fe–C5, 2.446 (2); Fe–B6, 2.319 (2); Fe–B7, 2.287 (2); C2–C5, 1.475 (3); C2–B4, 1.583 (3); B4–B7, 1.834 (4); C3–B7, 1.571 (3); C3–B6, 1.578 (3); Fe–C2a, 1.976 (2); Fe–C3a, 1.953 (2); Fe–B4a, 2.220 (2); Fe–C5a, 2.472 (2); Fe–B6a, 2.326 (2); Fe–B7a, 2.283 (2); C2a–C5a, 1.475 (3); C2a–B4a, 1.578 (3); B4a–B7a, 1.837 (3); C3a–B7a, 1.580 (3); C3a–B6a, 1.574 (3).

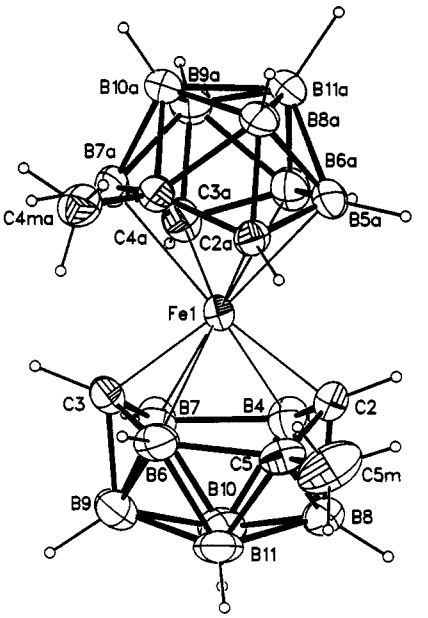

Figure 3. ORTEP drawing of the molecular structure of *commo-Fe*-(1-Fe-5-CH_3-2,3,5-$C_3B_7H_9$)(1-Fe-4-CH_3-2,3,4-$C_3B_7H_9$) (**8**). Selected bond distances (Å): Fe–C2, 1.987 (4); Fe–C3, 1.941 (3); Fe–B4, 2.215 (6); Fe–C5, 2.469 (5); Fe–B6, 2.320 (5); Fe–B7, 2.271 (5); C2–C5, 1.478 (6); C2–B4, 1.565 (6); B4–B7, 1.844 (7); C3–B7, 1.572 (7); C3–B6, 1.565 (7); Fe–C2a, 1.985 (4); Fe–C3a, 1.956 (5); Fe–B5a, 2.313 (4); Fe–C4a, 2.341 (4); Fe–B7a, 2.318 (5); Fe–B6a, 2.292 (5); C2a–C4a, 1.485 (6); C2a–B5a, 1.571 (6); B5a–B6a, 1.834 (7); C3a–B6a, 1.595 (6); C3a–B7a, 1.560 (7).

with the cages oriented in a cis conformation. Isomer **7** (Figure 2), *commo-Fe*-(1-Fe-5-CH_3-2,3,5-$C_3B_7H_9$)$_2$, is again composed of only one type of anion enantiomer (equal mixture of *RR* and *SS*), but the methyl has, as was observed in 1-(η-C_5H_5)Fe-4-CH_3-2,3,4-$C_3B_7H_9$ (**3**) in the preceding paper, "migrated" to the 4-vertex position. The

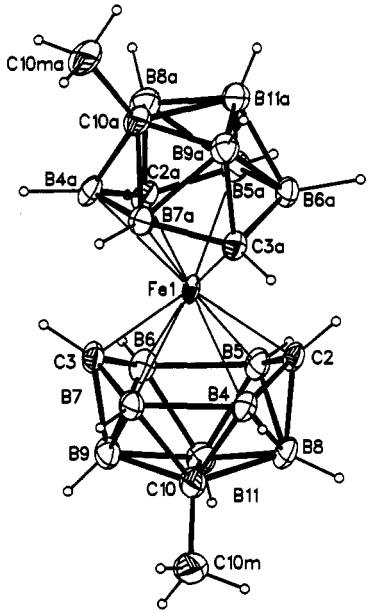

Figure 4. ORTEP drawing of the molecular structure of *commo-Fe*-(1-Fe-10-CH_3-2,3,10-$C_3B_7H_9)_2$ (**9**). Selected bond distances (Å): Fe–C2, 1.994 (5); Fe–C3, 2.001 (5); Fe–B4, 2.243 (7); Fe–B5, 2.360 (6); Fe–B6, 2.327 (6); Fe–B7, 2.257 (6); C2–B5, 1.573 (9); C2–B4, 1.548 (8); B4–B7, 1.831 (9); C3–B7, 1.553 (9); C3–B6, 1.553 (9); C10–B4, 1.758 (8); C10–B7, 1.743 (7); C10–B8, 1.679 (8); C10–B9, 1.699 (10); C10–B11, 1.777 (9); Fe–C2a, 1.986 (4); Fe–C3a, 1.978 (5); Fe–B4a, 2.259 (6); Fe–B5a, 2.342 (6); Fe–B6a, 2.302 (7); Fe–B7a, 2.285 (6); C2a–B5a, 1.563 (9); C2a–B4a, 1.560 (8); B4a–B7a, 1.825 (8); C3a–B7a, 1.567 (9); C3a–B6a, 1.558 (9); C10a–B4a, 1.746 (8); C10a–B7a, 1.712 (7); C10a–B8a, 1.685 (8); C10a–B9a, 1.683 (9); C10a–B11a, 1.777 (10).

two cages in **7** are oriented in a trans configuration. In *commo*-1-*Fe*-(5-CH_3-2,3,5-$C_3B_7H_9$)(4-CH_3-2,3,4-$C_3B_7H_9$) (**8**; Figure 3), the two cages are derived from the two different enantiomeric cages (*RS*) and again the methyl group on both cages has rearranged to the 4-vertex positions. The cages of **8** adopt a trans configuration.

The ratio of 6:7:8 produced in the original reaction was ~6:1:2. It was subsequently found that interconversions between these isomers could be effected thermally. Heating **6** produced **7** and **8**. Under certain conditions, **8** could be isolated in good yield; however, **7** could not be isolated without cogeneration of **8**. At lower temperatures the ratio of **7** to **8** was observed to be roughly 1:1, but at higher temperatures (240 °C) separate pure samples of **7** and **8** gave the same ratios (1:9) of 7:8, suggesting that these two isomers are in equilibrium at that temperature.

Thermolysis of **6**, **7**, or **8** at temperatures greater than 260 °C produced the final isomeric complex *commo-Fe*-(1-Fe-10-CH_3-2,3,10-$C_3B_7H_9)_2$ (**9**). A single-crystal structural determination of **9** (Figure 4) showed that the cage carbon present at the cage 4- (or 5-) position in **6**–**8** has rearranged in **9** to the cage 10-position. This configuration then achieves the maximum separation of the cage carbons and the maximum separation of the third carbon from the iron atom, in agreement with well-known trends in metallacarborane cage migrations.[8] In larger scale reactions small amounts of a red material which was found to be a mixture of two additional isomeric complexes was isolated, suggesting that other isomers may be intermediates in the conversion of **6**, **7**, or **8** to **9**. The possible mechanisms of these and the methyl "migration" rearrangements are discussed in the following paper.[9]

A comparison of the structures of **6**–**9** reveals several interesting features. As expected, the Fe atoms in these complexes have the strongest bonding interactions with the two four-coordinate carbons C2 and C3 in each cage and this interaction is enhanced when the methyl substituent has been replaced by a hydrogen. Thus, the Fe–C2(H) or Fe–C3(H) distances (average 1.972 Å) in **6**–**9** are shorter than the (Me)C2–Fe distance in **6** (2.021 (2) Å). A similar trend was observed in complexes **2** and **3** and in the cobaltatricarbaboranes **10** and **11**, which are discussed later.

In 1-(η-C_5H_5)Fe-(2-CH_3-2,3,4-$C_3B_7H_9$) (**2**), 1-(η-C_5H_5)-Fe-(4-CH_3-2,3,4-$C_3B_7H_9$) (**3**), and *commo-Fe*-(1-Fe-10-CH_3-2,3,10-$C_3B_7H_9)_2$ (**9**), the Fe sits reasonably centered in the tricarbon carborane face with the ferratricarbaborane adopting a gross octadecahedral geometry. However, in **6**–**8** significant cage distortions are observed. In **2** and **3**, the Fe–C4 distances ar 2.265 (3) and 2.282 (4) Å, respectively, but the corresponding Fe–C4 (or C5) distances in **6** (2.435 (3) Å), **7** (2.472 (2) and 2.446 (2) Å), and **8** (2.341 (5) and 2.469 (5) Å) are considerably lengthened. The net effect of this lengthening is to produce open four-membered Fe–C–C–B faces in each of the cages of **6** (Fe–C2–C5–B6), **7** (Fe–C2–C5–B6 and Fe–C2a–C5a–B6a), and **8** (Fe–C2–C5–B6 and Fe–C2a–C4a–B7). We previously noted a similar distortion in the nickel tricarbaborane compound 1-[η-$C_4(CH_3)_4H$]Ni-9,2,4-$(CH_3)_3$-2,3,4-$C_3B_7H_7$.[10]

Other 11-vertex metalladicarbaborane[11] complexes having a formal 24-skeletal-electron count have also exhibited cage distortions generating similar quadrilateral polyhedral faces, including 1-(η-MeC_6H_4-*i*-Pr)-2,4-Me_2-1,2,4-$RuC_2B_8H_8$ and 1,1-$(PPh_3)_2$-1-H-1,2,4-$IrC_2B_8H_{10}$. It is significant that the distortion in the above systems always leads to an open metal–C–C–B quadrilateral face that results from the lengthening of the metal–C4(5) bonding distances. When there is not a carbon in this position, such as in 1-(η-MeC_6H_4-*i*-Pr)-2,3-Me_2-1,2,3-$RuC_2B_8H_8$[11] or **9**, no distortion is observed. However, the presence of a carbon in the C4(5) position does not in itself mean that the cage will be distorted, as was seen in compounds **2** and **3**. Distortions to form even more open types of structures have been observed for other 11-vertex metalladicarbaboranes, including, for example, the compounds μ-10,8-$[(Me_3P)_2Pt]_2$-4,4-$[(Me_3P)_2]$-4,2,3-$PtC_2B_8H_{10}$,[12] 4,4-$[(Me_3P)_2]$-4,2,3-$PtC_2B_8H_{10}$, 7-H-7,3-$[(Et_3P)_2]$-7,2,4-$PtC_2B_8H_{10}$,[13] and 2-(η^6-C_6H_6)-8,10-Me_2-2,8,10-$OsC_2B_8H_8$.[14]

For 24-skeletal-electron clusters, the regular and distorted octadecahedral structures are apparently close in energy and any one of a number of factors may lead to a distortion. One factor that may be important in determining the cage geometry is the bonding abilities of the other ligands bound to the metal. For example, Mingos[15]

(8) (a) Williams, R. E. *Prog. Boron Chem.* **1970**, *2*, 37–118. (b) Williams, R. E. *Adv. Inorg. Chem. Radiochem.* **1976**, *18*, 67–142. (c) Dustin, D. F.; Evans, W. J.; Jones, C. J.; Wiersema, R. J.; Gong, H.; Chan, S.; Hawthorne, M. F. *J. Am. Chem. Soc.* **1974**, *96*, 3085–3090.

(9) Plumb, C. A.; Sneddon, L. G. *Organometallics*, following paper in this issue.

(10) Briguglio, J. J.; Sneddon, L. G. *Organometallics* **1986**, *5*, 327–336.

(11) (a) Bown, M.; Fontaine, X. L. R.; Greenwood, N. N.; Kennedy, J. D.; Thornton-Pett, M. *J. Chem. Soc., Dalton Trans.* **1990**, 3039–3049. (b) Bown, M.; Fontaine, X. L. R.; Greenwood, N. N.; Kennedy, J. D.; Thornton-Pett, M. *Organometallics* **1987**, *6*, 2254–2255. (c) Nestor, K.; Fontaine, X. L. R.; Greenwood, N. N.; Kennedy, J. D.; Plesek, J.; Stibr, B.; Thornton-Pett, M. *Inorg. Chem.* **1989**, *28*, 2219–2221.

(12) (a) Barker, G. K.; Green, M.; Spencer, J. L.; Stone, F. G. A.; Taylor, B. F.; Welch, A. J. *J. Chem. Soc., Chem. Commun.* **1975**, 804–805. (b) Green, M.; Spencer, J. L.; Stone, F. G. A. *J. Chem. Soc., Dalton Trans.* **1979**, 1679–1686.

(13) Barker, G. K.; Green, M.; Stone, F. G. A.; Wolsey, W. C.; Welch, A. J. *J. Chem. Soc., Dalton Trans.* **1983**, 2063–2069.

(14) Bown, M.; Fontaine, X. L. R.; Greenwood, N. N.; Kennedy, J. D.; Thornton-Pett, M. *J. Chem. Soc., Chem. Commun.* **1987**, 1650–1651.

has analyzed the origin of the slip distortions observed in platinacarboranes and suggested that they result from the nonconical nature of the $(PR_3)_2Pt$ fragment, which creates unequal bonding capabilities in the platinum d orbitals with respect to the cage. In this regard, complexes **2** and **3**, which have a conical CpFe fragment, are not distorted, but complexes **6–8**, which have two tricarbon carboranes bound to the irons, do exhibit significant cage-opening distortions. As a result of both the puckered tricarbon carborane metal-bonding face and the presence of the third carbon on this face, the frontier orbitals of a $(MeC_3B_7H_9Fe)$ fragment that could be used to bind to the second tricarbon carborane in **6–8** would be expected to be quite anisotropic and, on this basis, distortions in both cages of these complexes would be expected.

It should also be pointed out that the distorted structures observed for **6–8** may be of kinetic, rather than thermodynamic, origin. That is, an undistorted closo octadecahedron may, indeed, be the favored geometry for all isomers, and the observed distorted structures may be related to the mode of insertion of the iron ions into the cage. The distorted structures may then be trapped by, for example, a high steric barrier to their conversion to an undistorted structure. A similar behavior was observed in the rearrangements of 14-vertex diferracarboranes $(\eta\text{-}C_5H_5)Fe_2Me_4C_4B_8H_8$ from distorted to symmetrical isomers.[16]

The C2–C4(5) distances in the isomers are 1.478 (4) for **6**, 1.475 (3) and 1.475 (3) Å for **7**, and 1.478 (6) and 1.485 (6) Å for **8** and are somewhat shorter (~0.02–0.03 Å) than those observed in **2** and **3** but are in the range observed for carbon–carbon distances for adjacent carbons in analogous cage sites in 11-vertex metalladicarbaboranes.[10,11] Thus, the metal–C4(5) bond lengthening may result in an increase in the C2–C4(5) bonding. The remaining boron–boron and boron–carbon cage distances are within normal ranges.

Preliminary cyclic voltammetric studies of the major product **6** showed that the compound undergoes an irreversible oxidation at ~1.28 V. Thus, **6** shows significantly enhanced oxidation stability relative to both ferrocene Cp_2Fe (0.41 V) and the monocage compound **2** (0.79 V). A similar increase in oxidation stability was previously found[17] for the complexes $(1,2\text{-}CB_9H_{10}PMe)_2Fe$ (1.6 V) and $(1,7\text{-}CB_9H_{10}PMe)_2Fe$ (1.46 V), which are derived from another monoanionic carborane ligand, $CB_9H_{10}PMe^-$. Dicarbollide $(C_2B_9H_{11}^{2-})$ complexes generally have oxidation potentials lower than those of the corresponding metallocenes with the metal in the same oxidation state.[18] Therefore, in contrast to the dicarbollide ligand, which stabilizes high metal oxidation states, the monoanionic ligands $MeC_3B_7H_9^-$ and $CB_9H_{10}PMe^-$ tend to stabilize the metal 2+ oxidation state in these complexes.

The ^{11}B NMR spectra of **6** and **8** are similar, showing seven different resonances, and resemble those of compounds **2** and **3** in the preceding paper, which have the same cage structures. The CH resonances in the ^1H NMR spectra of **6**, **8**, and **9** (and **2** and **3**) proved to be diagnostic of their carbon framework positions. Protons or a methyl group bound to one of the four-coordinate carbons adjacent to the iron appeared downfield, while those bound to carbons in other positions appeared upfield. Thus in **6**, which has C3H and C5H groups, one CH resonance is observed at low field (6.56 ppm) and the other at high field (1.55 ppm), while **8** and **9**, which have hydrogens at both C2 and C3, each have two resonances at low field (**8**, 6.05 and 5.41 ppm; **9**, 5.79 and 5.55 ppm). Similarly the methyl resonance (C3) in **6** appears at 2.01 ppm, but in **8** (C5) and **9** (C5) they appear at 0.93 and 1.12 ppm, respectively.

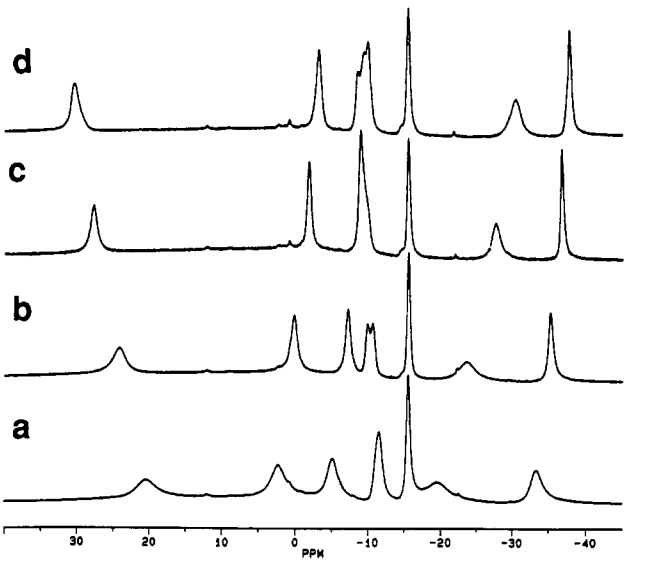

Figure 5. Variable-temperature 160-MHz ^{11}B NMR spectra for **7**: (a) 27 °C; (b) 50 °C; (c) 70 °C; (d) 90 °C.

The NMR spectra of *commo-Fe*-$(1\text{-Fe-}5\text{-}CH_3\text{-}2,3,5\text{-}C_3B_7H_9)_2$ (**7**) were unique, however, since they showed evidence of dynamic behavior. Both the ^1H and ^{11}B NMR spectra at room temperature exhibited only broad signals. The ^{13}C spectrum could not be observed. Variable-temperature studies were carried out over the range of −50 to +90 °C to investigate this process. As shown in Figure 5, the ^{11}B NMR spectra at 160 MHz were observed to sharpen and the resonances to shift apart with increasing temperature. This behavior suggests that at 90 °C the system may be approaching the fast exchange limit of a fluxional process. However, the resonances remained broad upon lowering the temperature and the sharp spectrum expected for a static structure could not be observed in the ^{11}B NMR experiments.

The resonances in the ^1H NMR spectra of **7** at 500 MHz are broad at room temperature but sharpen and shift with decreasing temperature. At −50 °C three sharp resonances are apparent, corresponding to the two CH groups (3.84 and 4.58 ppm) and the methyl group (1.95 ppm). The positions of these peaks were still changing with temperature, indicating that the compound is approaching, but has not yet attained, a static structure. As shown in Figure 6, when the temperature is increased above room temperature, the broad resonances again sharpen and shift, until at 90 °C seven sharp BH quartets along with a methyl and two CH resonances are observed. It is significant that, in the spectrum at 90 °C, the two CH resonances appear at high field (1.32 and −6.01 ppm) and the methyl–C5 resonance occurs at low field (9.53 ppm). These observations suggest that under the fast exchange conditions, the cage carbon atoms have very different metal-bonding interactions than in the static structure.

(15) (a) Mingos, D. M. P. *J. Chem. Soc., Dalton Trans.* **1977**, 602–610. (b) Mingos, D. M. P.; Forsyth, M. I.; Welch, A. J. *J. Chem. Soc., Dalton Trans.* **1978**, 1363–1634. (c) Evans, D. G.; Mingos, D. M. P. *J. Organomet. Chem.* **1982**, *240*, 321–327. (d) See also: O'Neill, M. E.; Wade, K. In *Metal Interactions in Boron Clusters*; Grimes, R. N., Ed.; Plenum: New York, 1980; pp 1–41.

(16) Maxwell, W. M.; Weiss, R.; Sinn, E.; Grimes, R. N. *J. Am. Chem. Soc.* **1977**, *99*, 4016–4029.

(17) Little, J. L.; Welcker, P. S.; Loy, N. J.; Todd, L. J. *Inorg. Chem.* **1970**, *9*, 63–69.

(18) Geiger, W. E., Jr. In *Metal Interactions with Boron Clusters*; Grimes, R. N., Ed.; Plenum Press: New York, 1982; Chapter 6, pp 239–268.

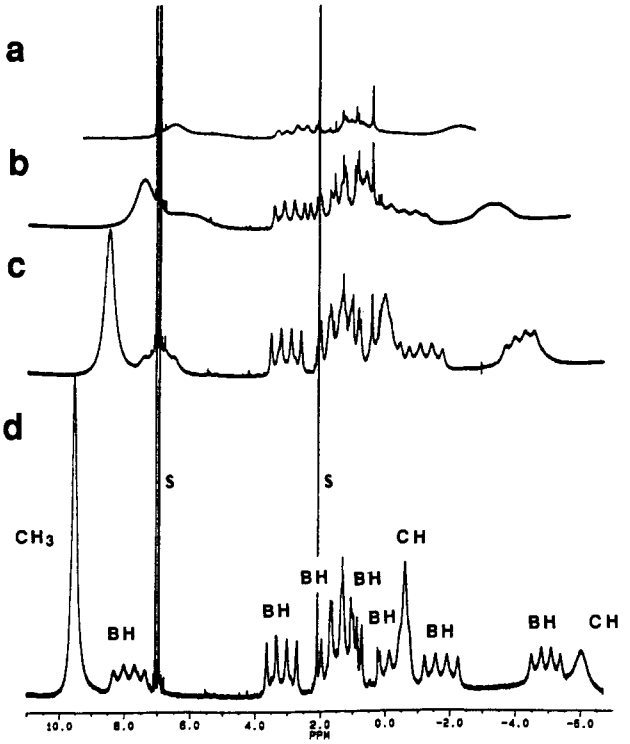

Figure 6. Variable-temperature 500-MHz ^1H NMR spectra for **7**: (a) 27 °C; (b) 50 °C; (c) 70 °C; (d) 90 °C.

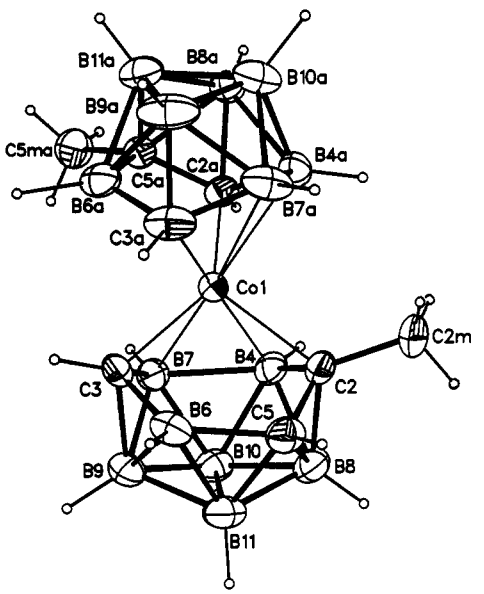

Figure 7. ORTEP drawing of the molecular structure of *commo-Co*-(1-Co-2-CH_3-2,3,5-$C_3B_7H_9$)(1-Co-5-CH_3-2,3,5-$C_3B_7H_9$) (**10**). Selected bond distances (Å): Co–C2, 2.072 (2); Co–C3, 1.962 (3); Co–B4, 2.232 (3); Co–C5, 2.604 (2); Co–B6, 2.443 (3); Co–B7, 2.271 (3); C2–C5, 1.458 (4); C2–B4, 1.589 (4); B4–B7, 1.886 (4); C3–B7, 1.548 (4); C3–B6, 1.586 (3); Co–C2a, 2.027 (2); Co–C3a, 1.964 (3); Co–B4a, 2.259 (3); Co–C5a, 2.615 (2); Co–B6a, 2.430 (3); Co–B7a, 2.314 (4); C2a–C5a, 1.458 (3); C2a–B4a, 1.574 (4); B4a–B7a, 1.879 (5); C3a–B7a, 1.553 (5); C3a–B6a, 1.591 (4).

Fluxional behavior has been previously observed in other 11-vertex polyhedral boranes, including $B_{11}H_{11}^{2-}$,[19] $CB_{10}H_{11}^-$,[20] $B_{11}Se_3H_9^{2-}$,[21] and 5-(η-C_5H_5)Co-(2-Me_3N-2-CB_9H_9).[22]

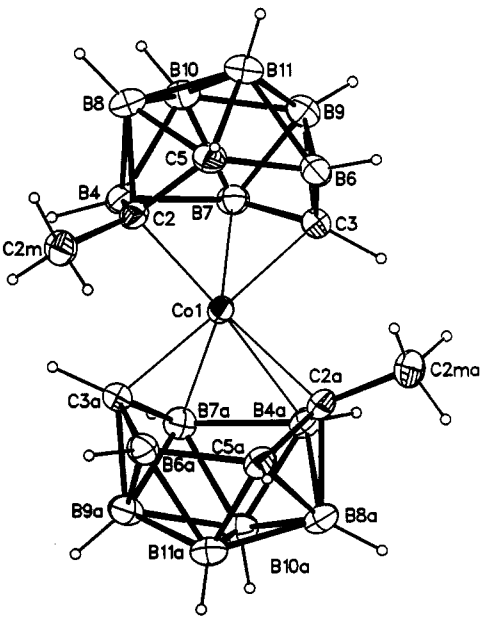

Figure 8. ORTEP drawing of the molecular structure of *commo-Co*-(1-Co-2-CH_3-2,3,5-$C_3B_7H_9$)$_2$ (**11**). Selected bond distances (Å): Co–C2, 2.068 (2); Co–C3, 1.990 (3); Co–B4, 2.256 (3); Co–C5, 2.655 (2); Co–B6, 2.546 (3); Co–B7, 2.300 (3); C2–C5, 1.481 (3); C2–B4, 1.597 (4); B4–B7, 1.882 (5); C3–B7, 1.566 (4); C3–B6, 1.585 (4); Co–C2a, 2.070 (2); Co–C3a, 1.981 (2); Co–B4a, 2.261 (3); Co–C5a, 2.670 (2); Co–B6a, 2.546 (3); Co–B7a, 2.312 (2); C2a–C5a, 1.478 (4); C2a–B4a, 1.594 (3); B4a–B7a, 1.880 (4); C3a–B7a, 1.566 (4); C3a–B6a, 1.581 (4).

The temperature dependence of the spectra reported for 5-(η-C_5H_5)Co-(2-Me_3N-2-CB_9H_9) also suggests that, as proposed for **7**, the compound is undergoing a slow exchange at room temperature. The diamond–square–diamond (dsd) and belt-rotation mechanisms[19,20] previously proposed to account for the dynamic behavior in 11-vertex closo polyhedra involve the opening and closing of open four-membered faces. The quadrilateral distortions observed in the complexes **6**–**8** may well be related to the transition states needed for these rearrangements.

Alternatively, the dynamic behavior observed for **7** may be related to metal–ligand rotational rearrangements. Kennedy has recently proposed[23] that the fluxional behavior observed in another 11-vertex platinacarborane, 1,1-$(PMe_2Ph)_2$-1,2,3-$PtC_2B_8H_9$-X (X = H, Me, Ph), is due to such rotational fluxionality and furthermore that these rearrangements are accompanied by a flexing of the $C_2B_8H_9X$ carborane framework between nido and arachno geometries.

Obviously, the details of the rearrangement process observed for **7** and the reason only **7**, but not **6**, **8**, or **9**, is fluxional remain to be determined.

Cobaltatricarbaborane Complexes 10 and 11. The reaction of $CoCl_2$ and 2 equiv of $Na^+(6\text{-}CH_3\text{-}5,6,9\text{-}C_3B_7H_9)^-$ produced two paramagnetic cobaltatricarbaborane isomers:

$$2Na^+(6\text{-}CH_3\text{-}5,6,9\text{-}C_3B_7H_9) \xrightarrow[-2NaCl]{CoCl_2} \underset{\mathbf{10}}{\textit{commo-Co}\text{-}(1\text{-}Co\text{-}2\text{-}CH_3\text{-}2,3,5\text{-}C_3B_7H_9)\text{-}(1\text{-}Co\text{-}5\text{-}CH_3\text{-}2,3,5\text{-}C_3B_7H_9)} + \underset{\mathbf{11}}{\textit{commo-Co}\text{-}(1\text{-}Co\text{-}2\text{-}CH_3\text{-}2,3,5\text{-}C_3B_7H_9)_2} \quad (2)$$

(19) (a) Tolpin, E. I.; Lipscomb, W. N. *J. Am. Chem. Soc.* **1973**, *95*, 2384–2386. (b) Muetterties, E. L.; Hoel, E. L.; Salentine, C. G.; Hawthorne, M. F. *Inorg. Chem.* **1975**, 950–951. (c) Kleier, D. A.; Dixon, D. A.; Lipscomb, W. N. *Inorg. Chem.* **1978**, *17*, 166–176.

(20) Wiersema, R. J.; Hawthorne, M. F. *Inorg. Chem.* **1973**, *12*, 785–788.

(21) Friesen, G. D.; Little, J. L.; Huffman, J. C.; Todd, L. J. *Inorg. Chem.* **1979**, *18*, 755–758.

(22) Schultz, R. V.; Huffman, J. C.; Todd, L. J. *Inorg. Chem.* **1979**, *18*, 2883–2886.

(23) Kennedy, J. D.; Thornton-Pett, M.; Stibr, B.; Jelinek, T. *Inorg. Chem.* **1991**, *30*, 4481–4484.

The paramagnetism of **10** and **11** precluded characterization by NMR techniques, but single-crystal X-ray determinations established the structures of both compounds, as shown in the ORTEP drawings in Figures 7 and 8.

Like the ferratricarbaboranes, both **10** and **11** are sandwich complexes. In *commo-Co*-(1-Co-2-CH_3-2,3,5-$C_3B_7H_9$)(1-Co-5-CH_3-2,3,5-$C_3B_7H_9$) (**10**), two different tricarbon carborane cage structures are present. In one cage, the methyl-substituted carbon is at the C2 vertex, while in the other cage, the methyl-substituted carbon is at the C5 vertex. The tricarbon carborane cages are of the same enantiomeric types (equal mixture of *RR* and *SS*), and they have a trans orientation with respect to each other. In *commo-Co*-(1-Co-2-CH_3-2,3,5-$C_3B_7H_9)_2$ (**11**), both cages have the same enantiomeric form (equal mixture of *RR* and *SS*) with the methyl-substituted carbon at the C2 position and the cages oriented in a cis manner.

The experimentally determined effective magnetic moments for **10** and **11** indicate that both compounds, like cobaltocene, have low-spin 19-electron configurations with a single unpaired electron. Both **10** and **11** have complex EPR spectra owing to their low symmetry and coupling to ^{59}Co ($S = {}^7/_2$). In addition, the spectra of both compounds show evidence of several species. In **11** at least two different g_1 values can be defined at $g_1 \approx 2.251$ and $g_1 \approx 2.132$. The corresponding g_2 and g_3 values apparently overlap at $g_2 \approx 2.22$ and $g_3 \approx 1.98$. These species may be, for example, rotational isomers present in solution that are trapped in the frozen matrix. Isomer **10** has two different types of tricarbon carborane cages and, as a result, a much more complicated spectrum that prevents simple analysis of the Co splitting pattern.

As in the ferratricarbaborane complexes **2–9**, the cobalt atoms have their closest cage contacts at the four-coordinate C2 and C3 carbons, with the shortest distances being observed when there is hydrogen substitution: **10**, Co–C2Me = 2.072 (2) Å compared to Co–C2aH = 2.027 (2) Å, Co–C3H, –C3aH = 1.962 (2), 1.964 (3) Å; **11**, Co–C2Me, –C2aMe = 2.068 (2), 2.070 (2) Å, Co–C3H, –C3aH = 1.990 (3), 1.981 (2) Å.

Both **10** and **11** show significant cage distortions resulting from a lengthening of *both* the Co–C5(C5a) (**10**, 2.604 (2) and 2.615 (2) Å; **11**, 2.655 (2) and 2.670 (2) Å) and the Co–B6(B6a) (**10**, 2.443 (3) and 2.430 (3) Å; **11**, 2.546 (3) and 2.546 (3) Å) distances. In both complexes the Co is closer to the B4–B7 edge (average Co–B4 and –B7 distance 2.276 Å) than to the B6–C5 edge. Therefore, in contrast to the quadrilateral opening in the ferratricarbaboranes, the cobaltatricarbaboranes have puckered pentagonal open faces (**10**, Co–C2–C5–B6–C3 and Co–C2a–C5a–B6a–C3a; **11**, Co–C2–C5–B6–C3 and Co–C2a–C5a–B6a–C3a). These open faces differ from those observed for 11-vertex clusters having a formal nido skeletal-electron count such as *commo*-$Ni(B_{10}H_{12})^{2-}$,[24] $[Et_3P]_2Pt(H)SB_9H_{10}$,[25] $(C_2B_9H_{11})Co(C_2B_8H_{10}py)^-$,[26] and *commo-Pt*-(nido-1-Pt-2-CH_3-2,3,5-$C_3B_7H_9)_2$.[27] The nido compounds have structures based on an icosahedron missing one vertex and exhibit nearly planar five-membered open faces. The open faces of **10** and **11** are clearly nonplanar, and the structures appear to be intermediate between the normal 11-vertex closo (24-skeletal-electron) and nido (26-skeletal-electron) geometries. Such intermediate structures are, in fact, reasonably expected on the basis of skeletal-electron-counting relationships. Thus, the paramagnetic cobaltatricarbaboranes **10** and **11** have one more electron than the ferratricarbaboranes **1**, **2**, and **6–9**. If this extra electron is totally metal-centered, then closo-octadecahedral cage geometries, such as found in the ferratricarbaboranes, might be expected. However, if the extra electron is partially delocalized into the tricarbaborane ligands, then cage antibonding levels will be populated and a partial cage opening should result. Clearly the structures observed for **10** and **11** might be consistent with the latter case.

Surprisingly, both **10** and **11**, in contrast to cobaltocene, are air-stable and, in fact, could not be oxidized to the diamagnetic cobaltocenium analogue with any of the common oxidizing agents studied. Preliminary cyclic voltammetric studies of the major product **11** showed a well-defined reversible wave at 0.24 V (Co^I–Co^{II} redox couple) and an irreversible oxidation wave at ~0.91 V (Co^{II}–Co^{III} redox couple). In cobaltocene the Co^I–Co^{II} couple is observed at –1.88 V and the Co^{II}–Co^{III} couple is observed at –0.94 V. Thus, the Co^{II}–Co^{III} oxidation in **11** is ~1.8 V more positive than that of cobaltocene. This accounts for the air stability of these complexes, as well as their inertness toward the oxidizing agents studied. The isolation of a neutral, air-stable 19-electron cobalt complex is certainly unique in metallocene chemistry; however, Todd[17] has previously rported air-stable cobaltaphosphacarborane complexes containing the $CB_9H_{10}PMe^-$ ligand showing enhanced oxidative stabilities ((1,2-$CB_9H_{10}PMe)_2Fe$, 1.6 V; (1,7-$CB_9H_{10}PMe)_2Fe$, 1.46 V). These observations again demonstrate, as discussed above for the ferratricarbaboranes, the ability of the monoanionic tricarbon carboranes to stabilize the +2 metal oxidation state in these commo complexes.

In summary, although the development of polyhedral tricarbon carborane chemistry is still in its initial stages, it is clear on the basis of the work reported in this and the preceding paper that metal complexes derived from these carboranes may have properties that are complementary to the analogous cyclopentadienyl and dicarbollide systems. We are presently attempting to generate a range of new tricarbon carborane cage systems and derived metal complexes to investigate these possibilities.

Acknowledgment. We thank the National Science Foundation and the donors of the Petroleum Research Fund, administered by the American Chemical Society, for the support of this research. We also thank Dr. Alan Sherry and Gabriel Asturias for help with the EPR and electrochemical experiments.

Supplementary Material Available: Tables of hydrogen atom positional parameters, anisotropic temperature factors, bond distances, and bond angles for **6–11** (53 pages); tables of structure factors (74 pages). Ordering information is given on any current masthead page.

(24) Guggenberger, L. J. *J. Am. Chem. Soc.* **1972**, *94*, 114–119.
(25) Kane, A. R.; Guggenberger, L. J.; Muetterties, E. L. *J. Am. Chem. Soc.* **1970**, *92*, 2571–2572.
(26) Churchill, M. R.; Gold, K. *Inorg. Chem.* **1973**, *12*, 1157–1165.
(27) (a) Barnum, B.; Plumb, C. A.; Carroll, P. J.; Sneddon, L. G. Abstracts of Papers, BORON-USA II Meeting, Raleigh, NC, 1990. (b) Barnum, B.; Carroll, P. J.; Sneddon, L. G. Manuscript in preparation.